The Influence of Wave– and Zonal Mean–Ozone Feedbacks on the Quasi-biennial Oscillation

EUGENE C. CORDERO

Cooperative Research Centre for Southern Hemisphere Meteorology, Monash University, Clayton, Victoria, Australia

TERRENCE R. NATHAN

Atmospheric Science Program, Department of Land, Air and Water Resources, University of California, Davis, Davis, California

(Manuscript received 9 August 1999, in final form 6 March 2000)

ABSTRACT

The effects of wave and zonal mean ozone heating on the evolution of the quasi-biennial oscillation (QBO) are examined using a two-dimensional mechanistic model of the equatorial stratosphere. The model atmosphere is governed by coupled equations for the zonal mean and (linear) wave fields of ozone, temperature, and wind, and is driven by specifying the amplitudes of a Kelvin wave and a Rossby–gravity wave at the lower boundary. Wave–mean flow interactions are accounted for in the model, but not wave–wave interactions.

A reference simulation (RS) of the QBO, in which ozone feedbacks are neglected, is carried out and the results compared with *Upper Atmosphere Research Satellite* observations. The RS is then compared with three model experiments, which examine separately and in combination the effects of wave ozone and zonal mean ozone feedbacks. Wave–ozone feedbacks alone increase the driving by the Kelvin and Rossby–gravity waves by up to 10%, producing stronger zonal wind shear zones and a stronger meridional circulation. Zonal mean–ozone feedbacks (ozone QBO) alone decrease the magnitude of the temperature QBO by up to 15%, which in turn affects the momentum deposition by the wave fields. Overall, the zonal mean–ozone feedbacks increase the magnitude of the meridional circulation by up to 30%. The combined effects of wave–ozone and ozone QBO feedbacks generally produce a larger response then either process alone. Moreover, these combined ozone feedbacks produce a temperature QBO amplitude that is up to 30% larger than simulations without the feedbacks. Correspondingly, significant changes are also observed in the zonal wind and ozone QBOs. When ozone feedbacks are included in the model, the Kelvin and Rossby–gravity wave amplitudes can be reduced by ~10% and still produce a QBO similar to simulations without ozone.

1. Introduction

The quasi-biennial oscillation (QBO) of the zonal mean wind is one of the most striking circulation features of the lower equatorial stratosphere. The QBO was discovered independently by Reed et al. (1961) and Veryard and Ebdon (1961), and shortly thereafter, Funk and Garnham (1962) and Ramanathan (1963) identified a QBO in total-column ozone. Because the QBO plays a central role in the natural variability of ozone and other stratospheric trace gases, understanding the processes that affect its evolution is crucial for assessing the relative importance of natural versus anthropogenically induced ozone variability.

Historically, numerical modeling studies of the QBO have generally focused on the dynamical processes responsible for the zonal mean QBO and have largely neglected the potentially important feedbacks of ozone heating. Such feedbacks have been neglected despite evidence showing that the ozone heating produced by both wave motions and the zonal mean meridional circulation can affect the temperature structure of the equatorial lower stratosphere.

Echols and Nathan (1996) demonstrate, for example, that wave–ozone interactions have an important effect on the Kelvin wave induced zonal mean body force in the lower equatorial stratosphere. They show that ozone–dynamics interactions can significantly enhance the Kelvin wave amplitudes, resulting in a ~30% increase in the Eliassen–Palm (EP) flux divergence. Cordero et al. (1998) extended Echols and Nathan's study by incorporating the Kelvin wave–ozone feedbacks as well as those due to Rossby–gravity waves into a one-dimensional (1D) model of the QBO. They show that the ozone heating feedbacks modify the Kelvin and Rossby–gravity waves producing a ~10% increase in

Corresponding author address: Dr. Eugene C. Cordero, CRC Meteorology, Monash University, Clayton, Vic 3168, Australia.
E-mail: ecc@vortex.shm.monash.edu.au

the QBO amplitude and a ~2-month increase in its oscillation period. Cordero et al.'s study clearly demonstrates the importance of wave–ozone heating on the QBO, but the simplicity of their model precluded examining how either the meridional wave structure or changes in the zonal mean–ozone distribution feedback and affect the zonal mean circulation.

In addition to the wave–ozone feedbacks cited above, zonal mean–ozone feedbacks also play an important role in the QBO. This point was recognized by Dunkerton (1985), who suggested that ozone advection associated with the ozone QBO may produce enhanced local heating, resulting in a change in the zonal mean meridional circulation. To examine the effects of zonal mean–ozone feedbacks on the QBO, recent studies (Hasebe 1994; Li et al. 1995; Huang 1996) have employed two-dimensional (2D) models in which the QBO is driven by means other than the momentum deposition associated with the wave fields. For example, using a 2D model in which the QBO is prescribed by observed equatorial winds, Hasebe asserts that the zonal mean ozone distribution is responsible for the observed out of phase relationship between the zonal wind and ozone QBOs (ozone leads the zonal wind by ~¼ period). Hasebe also asserts that the omission of the zonal mean feedback may lead to an overestimation of the vertical velocity and may partially explain the deficiency of easterly momentum in the QBO momentum budget (Lindzen and Tsay 1975). Using a model in which the QBO is relaxed toward observed equatorial winds, Li et al. (1995) present additional evidence showing that the ozone QBO has an important effect on the temperature and wind structure of the equatorial stratosphere. In contrast, however, Huang (1996) uses a 2D model including prescribed QBO wave driving, to show that the ozone radiative feedbacks due to the ozone QBO have little effect on the meridional circulation and ozone field. Additional studies are clearly needed to fully resolve this issue. Finally, we stress that in Hasebe's, Li et al.'s, and Huang's models the QBO is *not* explicitly driven by wave motions. Thus, the effects of wave ozone feedbacks on the zonal wind and ozone QBOs could not be addressed in their models.

Ozone heating feedbacks clearly have a significant influence on the zonal mean QBO. Yet, despite their importance, no mechanistic study has thus far been carried out to study and quantify the *combined* effects of wave–ozone and zonal mean–ozone feedbacks on the evolution of the QBO. Addressing this problem forms the basis of the work presented here. In particular, our main objective is to investigate the influence of ozone–dynamics interactions on the zonal wind and ozone QBOs using a 2D model of the lower equatorial stratosphere. Two key questions are addressed here. How do ozone-induced wave changes affect the tropical stratospheric circulation? What influence do the diabatic feedbacks of the ozone QBO have on the dynamical QBO, and can these feedbacks account for some of the ''missing'' momentum in the simulations of the momentum budget of the QBO? Answers to these questions will help clarify the role ozone plays in the QBO and may provide additional insight into why QBO-like circulations are often absent in general circulation models.

The paper is organized as follows. Section 2 briefly describes the observed characteristics and theory of the zonal wind and ozone QBOs. Section 3 describes the model equations, basic states, and radiative–photochemical parameterizations. Section 4 presents a reference simulation (RS) of the QBO, where ozone feedbacks are neglected, and compares the results with *Upper Atmosphere Research Satellite* (*UARS*) observations. Section 5 compares the RS with the results of experiments that examine separately and in combination the effects of wave–ozone and zonal mean–ozone (ozone QBO) feedbacks. The summary and conclusions are presented in section 6.

2. Characteristics and theory of the QBO

a. Zonal wind QBO

Observations of the lower equatorial stratosphere reveal the unique time, height, and latitude variations of the QBO (Wallace 1973; Dunkerton and Delisi 1985; Naujokat 1986). The wind patterns are irregular, with periods ranging from 22 to 34 months and a mean period of ~28 months. The easterly winds are generally stronger than the westerly winds, with maximum wind speeds over the equator near the 26-km level. Westerly wind regimes persist longer than easterly wind regimes at lower levels; easterly winds remain longer than westerly winds at upper levels. The oscillation has a meridional extent of about 15° latitude and has little zonal variation (Andrews et al. 1987). The QBO is nearly symmetric about the equator, except in the middle atmosphere near the solstices (Dunkerton and Delisi 1997).

A theoretical explanation for the QBO, which was originally developed by Lindzen (1971) and Holton and Lindzen (1972), is that the momentum deposition associated with damped vertically propagating equatorial waves drives the zonal mean flow. Holton and Lindzen used a simple 1D model to demonstrate how thermally and mechanically damped Kelvin and Rossby–gravity waves can produce zonal mean flow variations that resemble many of the observed characteristics of the zonal wind QBO. Although later two- and three-dimensional simulations of the QBO support the Holton and Lindzen theory, several unresolved problems remain. For example, observations reveal that Kelvin and Rossby–gravity waves alone do not possess the momentum flux necessary to drive the observed zonal mean circulation (Lindzen and Tsay 1975; Salby et al. 1984; Takahashi and Boville 1992). This is especially true for the Rossby–gravity wave, which appears only intermittently in observations. Investigations into other momentum sources that contribute to the driving of the QBO include

laterally propagating Rossby waves (Dunkerton 1983) and westward-propagating gravity waves (Takahashi and Holton 1991). Gravity waves have been suggested as a possible source of both easterly and westerly momentum (Dunkerton 1997), although their precise role in the QBO has yet to be determined.

b. Ozone and temperature QBOs

Because ozone is largely controlled in the lower stratosphere by dynamics and in the mid- to upper stratosphere by temperature-dependent photochemistry, its natural variability is intimately connected to the QBO. In fact, analysis of satellite data reveals an ozone QBO whose spatial and temporal structure is more complicated than previously thought (Bowman 1989; Hollandsworth et al. 1995; Tung and Yang 1994; Cordero et al. 1997).

As first pointed out by Reed (1964), because the temperature QBO is symmetric about the equator and has a phase reversal at about $\pm 15^\circ$ latitude, thermal wind balance in the westerly (easterly) shear zones of the QBO requires warm (cold) anomalies at the equator. Maintenance of this temperature anomaly against radiative damping results in a secondary meridional circulation that produces sinking (rising) motion in the westerly (easterly) shear zones near the equator. Because the vertical gradient of ozone volume mixing ratio is positive in the lower stratosphere, the vertical motions associated with the westerly (easterly) phase of the QBO produce positive (negative) ozone anomalies near the equator. A QBO is also seen in the total-column ozone field (Hollandsworth et al. 1995).

The vertical structure of the ozone QBO has been analyzed using ozone profiles from satellite observations. The Stratospheric Aerosol and Gas Experiment (SAGE II) reveals significant ozone anomalies in the equatorial region of the lower stratosphere (20–27 km) and middle stratosphere (30–38 km), with a node near 28 km (Zawodny and McCormick 1991; Hasebe 1994; Randel and Wu 1996). An analysis of the vertical ozone profiles from the Halogen Occultation Experiment (HALOE) shows a similar structure of the ozone QBO, although the node between the lower- and middle-stratosphere QBO variations is located near 30 km in altitude (Cordero et al. 1997). Significant QBO variations in tropical nitrogen dioxide (NO_2) were also noted in the SAGE II observations. A further modeling study by Chipperfield et al. (1994) demonstrates that the two-cell ozone QBO structure is due to ozone advection in the lower stratosphere and chemistry associated with reactive nitrogen (NO_y) in the middle stratosphere.

3. Model description

The dynamics of the 2D model used here is based on Takahashi (1987). Briefly, the model atmosphere, which accounts for wave–mean but not wave–wave interactions, is represented by zonal mean and linear wave descriptions of the primitive equations. Specifying the geopotential height of both a Kelvin wave and a Rossby–gravity wave at the lower boundary drives the model circulation. Takahashi's model captures the essential characteristics of the QBO in the lower stratosphere and yields results that are qualitatively similar to Takahashi and Boville's (1992) three-dimensional QBO simulation.

We extend Takahashi's (1987) model to include the diabatic effects of both wave and zonal mean–ozone heating as follows. Perturbation (wave) and zonal mean ozone continuity equations are coupled via the diabatic heating to the perturbation and zonal mean temperature equations, respectively. Therefore, the model is capable of simulating the zonal wind, temperature, and ozone QBOs below 30 km and can account for how changes in the wave fields influence the zonal mean circulation. Processes that influence the QBO above 30 km, such as chemical feedbacks and the interaction between the QBO and semiannual oscillation, are not captured by our model.

a. Governing equations

The governing equations, which consist of momentum in the zonal and vertical directions, mass continuity, temperature, and ozone continuity, are represented on an equatorial beta plane in log-pressure coordinates, where $z = -H \ln(p/p_s)$; $H = 7$ km is the scale height and p_s is the surface pressure. All dependent variables are partitioned into a zonal mean (denoted with overbars) and two wave components (denoted with primes), a wave-1 ($k = 1$) Kelvin wave and a wave-4 ($k = 4$) Rossby–gravity wave. These zonal wavenumbers are consistent with other modeling studies (Takahashi 1987; Takahashi and Boville 1992) and observations (Yanai and Maruyama 1966; Wallace and Kousky 1968).

Zonal mean equations:

$$\frac{\partial \overline{u}}{\partial t} + \overline{v}\frac{\partial \overline{u}}{\partial y} + \overline{w}\frac{\partial \overline{u}}{\partial z} - \beta y \overline{v} = -\frac{\partial}{\partial y}(\overline{u'v'}) - \frac{1}{\rho}\frac{\partial}{\partial z}(\overline{\rho u'w'}) + \nabla_D^2 \overline{u}, \quad (1)$$

$$\frac{\partial \overline{v}}{\partial t} + \beta y \overline{u} = -\frac{\partial \overline{\Phi}}{\partial y} + \nabla_D^2 \overline{v}, \quad (2)$$

$$\frac{\partial \overline{v}}{\partial y} + \frac{1}{\rho}\frac{\partial(\rho \overline{w})}{\partial z} = 0, \quad (3)$$

$$\frac{\partial\overline{\Phi}_z}{\partial t}+\overline{v}\frac{\partial\overline{\Phi}_z}{\partial y}+\overline{w}\frac{\partial\overline{\Phi}_z}{\partial z}+N^2\overline{w}=-\frac{\partial}{\partial y}(\overline{v'\Phi'_z})-\alpha_N(\overline{\Phi}_z)+A\overline{\gamma}+\nabla_D^2\overline{\Phi}_z, \quad (4)$$

$$\frac{\partial\overline{\gamma}}{\partial t}+\overline{v}\frac{\partial\overline{\gamma}}{\partial y}+\overline{w}\frac{\partial\overline{\gamma}}{\partial z}=-\frac{\partial}{\partial y}(\overline{v'\gamma'})-\frac{1}{\rho}\frac{\partial}{\partial z}(\rho\overline{w'\gamma'})-B\overline{\gamma}-C\overline{\Phi}_z. \quad (5)$$

Wave equations:

$$\left(\frac{\partial}{\partial t}+\overline{u}\frac{\partial}{\partial x}\right)u'+v'\frac{\partial\overline{u}}{\partial y}+w'\frac{\partial\overline{u}}{\partial z}-\beta yv'=-\frac{\partial\Phi'}{\partial x}-\alpha_R u'+\nabla_D^2u', \quad (6)$$

$$\left(\frac{\partial}{\partial t}+\overline{u}\frac{\partial}{\partial x}\right)v'+\beta yu'=-\frac{\partial\Phi'}{\partial y}-\alpha_R v'+\nabla_D^2v', \quad (7)$$

$$\frac{\partial u'}{\partial x}+\frac{\partial v'}{\partial y}+\frac{1}{\rho}\frac{\partial(\rho w')}{\partial z}=0, \quad (8)$$

$$\left(\frac{\partial}{\partial t}+\overline{u}\frac{\partial}{\partial x}\right)\Phi'_z-v'\frac{\partial\overline{\Phi}_z}{\partial y}+N^2w'=-\alpha_N\Phi'_z+A\gamma'+\nabla_D^2\Phi'_z, \quad (9)$$

$$\left(\frac{\partial}{\partial t}+\overline{u}\frac{\partial}{\partial x}\right)\gamma'+v'\frac{\partial\overline{\gamma}}{\partial y}+w'\frac{\partial\overline{\gamma}}{\partial z}=-B\gamma'-C\Phi'_z-\alpha_R\gamma'+\nabla_D^2\gamma'. \quad (10)$$

The geopotential Φ is related to the temperature by $T=(H/R)\partial\Phi/\partial z$. The dissipation operator, ∇_D^2, is given by

$$\nabla_D^2=\nu\frac{\partial^2}{\partial z^2}+\kappa\left(\frac{\partial^2}{\partial x^2}+\frac{\partial^2}{\partial y^2}\right), \quad (11)$$

where ν and κ are the vertical and horizontal diffusion coefficients, respectively; the remaining symbols appearing in (1)–(10) have their standard meteorological meanings (see Table 1).

TABLE 1. List of symbols.

$x, y, z=-H\ln(p/p_0)$	Eastward, northward, and vertical directions
p_0	Sea level reference pressure
H	Density scale height
$\rho(z)=\rho_0\exp(-z/H)$	Basic-state density
ρ_0	Mean sea level density
β	Northward gradient of the Coriolis parameter evaluated at the equator
$\overline{u}(z)$, $\overline{T}(z)$, $\overline{\gamma}(z)$	Basic-state zonal mean wind, temperature, and ozone mixing ratio
$N^2(\overline{T})$	Brunt–Väisälä frequency squared
$u'(x, y, z, t)$, $v'(x, y, z, t)$	Zonal, meridional, and vertical wind components
$w'(x, y, z, t)$	Perturbation vertical wind component
$T'(x, y, z, t)$	Perturbation temperature
$\Psi'(x, y, z, t)$	Perturbation geopotential
$\gamma'(x, y, z, t)$	Perturbation ozone volume mixing ratio
$\alpha_N(z)$	Newtonian cooling coefficient
$\alpha_R(z)$	Raleigh friction
$A(z; \overline{T}, \overline{\gamma})$	Ozone heating coefficient
$B(z; \overline{T}, \overline{\gamma})$, $C(z; \overline{T}, \overline{\gamma})$	Radiative–photochemical coefficients in the ozone continuity equation

b. Boundary conditions

At the upper boundary ($z_t=34$ km) we set $\overline{w}=\overline{u}_z=\overline{v}_z=\overline{\Phi}_z=0$. At the lower boundary ($z_b=17$ km) we set $\overline{u}=\overline{v}=\overline{\Phi}=\overline{\Phi}_z=0$; $\overline{w}$ is solved for explicitly at the lower boundary by integrating the continuity equation (3) downward from the upper boundary. The geopotential heights for the Kelvin and Rossby–gravity waves at the lower boundary are

$$\Phi'_K=A_K\exp(-\beta y^2/2c_K)\,\mathrm{Re}[\exp ik_K(x-c_Kt)], \quad (12)$$

$$\Phi'_R=A_Ry\left(\frac{\beta m_R}{N}\right)^{1/2}\exp\left(-\frac{\beta|m_R|y^2}{2N}\right)\times\mathrm{Re}[\exp ik_R(x-c_Rt)], \quad (13)$$

where the subscripts K and R refer to the Kelvin and Rossby–gravity waves, respectively; (c_K, c_R) are the phase speeds; (k_K, k_R) are the zonal wavenumbers; (m_K, m_R) are the vertical wavenumbers; and (A_K, A_R) are the specified wave amplitudes. From (12) and (13), wave solutions at the lower boundary can be obtained for v', w', T', γ' (see appendix).

In the meridional direction the model domain extends from the equator to ±4500 km ($\sim\pm40°$ latitude). Symmetry about the equator is assumed for all zonal mean and wave fields, except the meridional motion of the Rossby–gravity wave, which is antisymmetric about the equator. Because the Kelvin and Rossby–gravity waves are equatorially trapped, we assume that sufficiently far from the equator all zonal mean and wave fields are zero ($u=v=\Phi_z=\gamma=0$).

c. Basic states and radiative–photochemical parameterizations

The initial temperature and ozone distributions used in the radiative and photochemical calculations are constructed from profiles representative of the September equinox. The temperature distribution shown in Fig. 1a is derived from the dataset of Fleming et al. (1988). The ozone volume mixing ratio distribution shown in Fig. 1b is from McPeters et al. (1984) from 17 to 27 km and from Keating et al. (1985) above 27 km. The ozone and

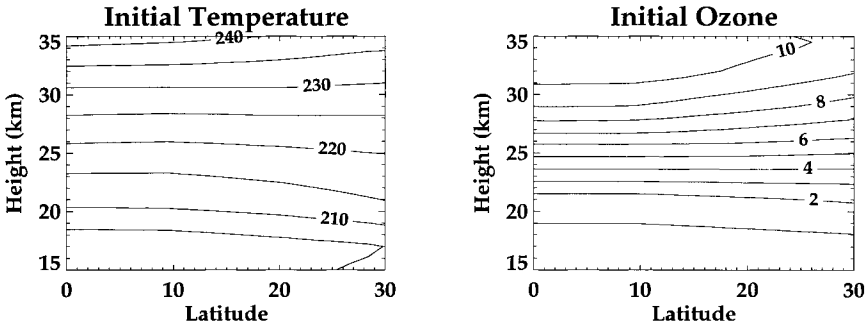

FIG. 1. Basic-state distribution of (a) zonal mean temperature, $\overline{T}$ (contour interval 5 K); and (b) zonal mean–ozone volume mixing ratio, $\overline{\gamma}$ (contour interval 1 ppmv).

temperature data are initialized to the model grid using a cubic spline interpolation routine.

The temporal evolution and spatial distribution of the ozone volume mixing ratios for the zonal mean and wave fields are governed by Eqs. (5) and (10), respectively. Because the wave transport terms in the ozone continuity Eq. (5) have relatively little effect on the ozone QBO (Ling and London 1986), they are hereafter neglected. In the absence of dynamical motions, the ozone fields relax to zero. Thus the modeled zonal mean ozone and temperature fields represent departures from their annual mean distributions.

Shown in Figs. 2a–c are the latitude–height distributions of the radiative–photochemical coefficients, *A*, *B*, and *C*, which are calculated using the reference temperature and ozone distributions, and a latitude-dependent solar zenith angle representative of the September equinox. The parameterization for the ozone heating coefficient, *A*, is similar to that of Hartmann and Garcia (1979) and is explained in detail in Nathan (1989) and Nathan and Li (1991). The photochemical relaxation parameters, *B* and *C*, are calculated using the parameterization of Stolarski and Douglass (1985), which explicitly accounts for the ozone and temperature dependencies of catalytic cycles involving odd nitrogen, odd hydrogen, and chlorine species. Although the modeling of ozone is simple, it contains the essential processes necessary to describe the time evolution of the zonal mean and perturbation ozone fields (Zhu and Holton 1986; Nathan et al. 1994; Echols and Nathan 1996; Cordero et al. 1998).

d. Model parameters

The coefficients for Raleigh friction, $\alpha_R(z)$, and Newtonian cooling, $\alpha_N(z)$, are chosen of the form

$$\begin{pmatrix}\alpha_R(z)\\ \alpha_N(z)\end{pmatrix} = \begin{pmatrix}5 \times 10^{-7}\ \mathrm{s}^{-1}\\ 7 \times 10^{-7}\ \mathrm{s}^{-1}\end{pmatrix} + 10^{-5}\ \mathrm{s}^{-1} \exp[5 \times 10^{-4}\,(z - z_t)]. \quad (14)$$

The Raleigh friction coefficient is identical to Takahashi's (1987). The Newtonian cooling coefficient is similar to Fels's (1982), which was calculated using radiative transfer rates that are dependent on the wave spatial scale. The increasing magnitudes of the Raleigh friction and Newtonian cooling coefficients toward the upper levels of the model are chosen to prevent spurious wave reflections off the top boundary. To preserve numerical stability, Raleigh friction is only applied to the wave fields.

The values for the horizontal and vertical viscosity coefficients, which are discussed in detail in Takahashi (1987), are $\kappa = 500\ \mathrm{m}^2\ \mathrm{s}^{-1}$ and $\nu = 0.04\ \mathrm{m}^2\ \mathrm{s}^{-1}$, respectively.

The values for the wave parameters in (12) and (13) are similar to those used in Takahashi and Boville's (1992) 3D model. For the Kelvin wave $c_K = 30\ \mathrm{m\ s}^{-1}$, $k_K = 1$, and $A_K = 300\ \mathrm{m}^2\ \mathrm{s}^{-2}$, and for the Rossby–gravity wave $c_R = -30\ \mathrm{m\ s}^{-1}$, $k_R = 4$, and $A_R = 204\ \mathrm{m}^2\ \mathrm{s}^{-2}$.

In the numerical simulations presented below, the meridional and vertical grid resolutions are, respectively, 300 km (~2.7° latitude) and 0.5 km. The initial condition is a motionless atmosphere, and all of the model simulations are run in a perpetual equinox condition; that is, seasonal variations are not included in the model.

4. QBO reference simulation (ozone dynamics interactions omitted)

In this section we carry out an RS of the zonal wind, temperature, and ozone QBOs, where ozone feedbacks are neglected, corresponding to $A = 0$ in both (4) and (9). This RS, which is compared with *UARS* observations, will serve as a basis for comparison with the model experiments incorporating ozone dynamics interactions, which are described in section 5.

a. Zonal wind QBO

Figure 3a shows the time–height cross section of the zonal wind near the equator. The maximum winds are located between ~23- and ~26-km altitude, and vary between ~−30 and ~25 m s^{-1}, a range of 55 m s^{-1}. The easterly winds are stronger than the westerly winds

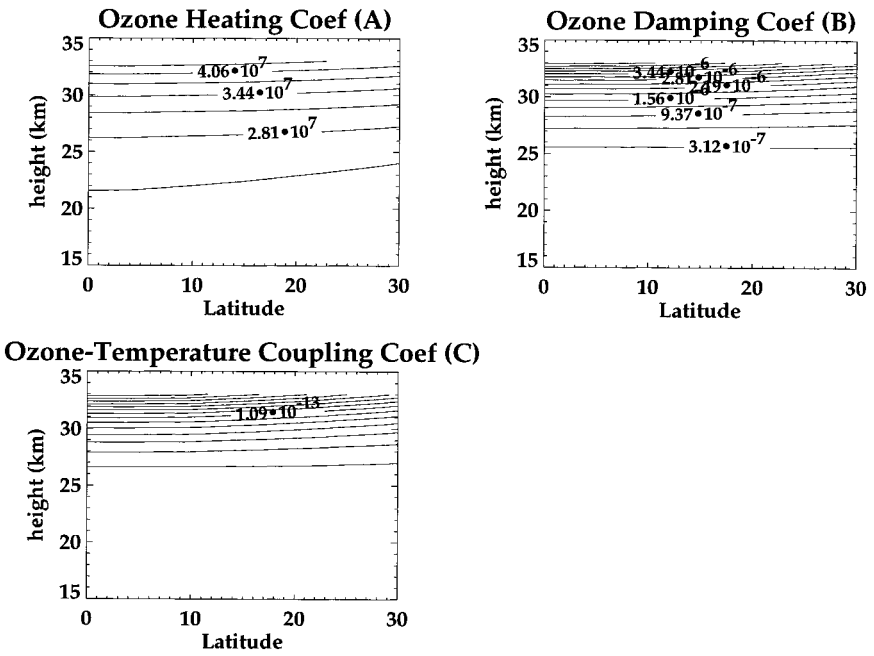

FIG. 2. Distribution of the (a) local ozone heating coefficient, A (contour interval 0.3 m s^{-3}); (b) ozone damping coefficient, B (contour interval 3.0 s^{-1} $\times$ 10^{-7}); and (c) ozone–temperature coupling coefficient C (contour interval 0.3 s m^{-1} $\times$ 10^{-12}).

and persist longer at higher levels. The westerly winds persist longer at lower levels; between ~20 and ~30 km, the westerly winds descend more rapidly than the easterly winds. The location and strength of the model winds agree well with Naujokat's (1986) observations showing maximum easterly winds of ~30 m s^{-1} at 26 km and maximum westerly winds of ~15 m s^{-1} at 24 km.

To facilitate comparison of the dominant modes of variability of the model, a power spectrum analysis of the model output is computed for each experiment. The power spectra are computed by calculating the amplitude of the discrete complex Fourier transform of the time series. The zonal wind power spectrum over the equator, which is displayed in Fig. 3b, shows a primary peak of 13 m s^{-1} at 26 months near 25-km altitude. Strong vertical wind shears exist at both the top and bottom boundaries, with the QBO signature maximized between 19- and 32-km altitude. The amplitude and period of the modeled QBO are very similar to observations made by the *UARS* High Resolution Doppler Imager (HRDI) instrument (Cordero et al. 1997). The dominant period of variability remains constant with latitude, whereas the amplitude rapidly diminishes (~8 m s^{-1} at 7.5° and only ~4 m s^{-1} at 12°). At the equator, a small-amplitude peak near 12 months, which is associated with a harmonic of the QBO frequency, is also evident.

b. Temperature QBO

The time–height structure of the zonal mean temperature QBO is displayed in Fig. 4. The temperature anom-

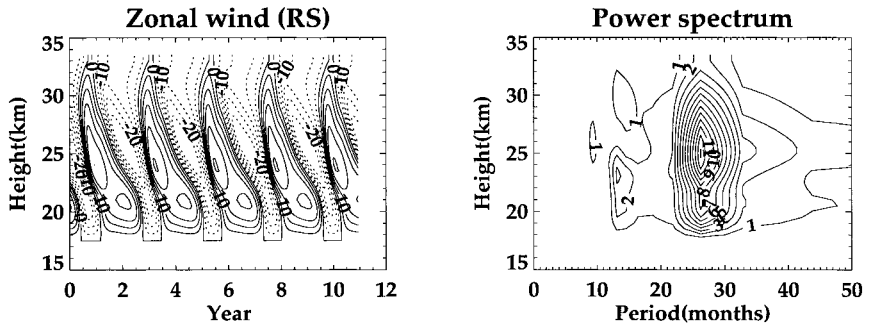

FIG. 3. (a) Time–height cross section of the zonal wind at the equator for the RS. Contour interval is 5 m s^{-1}, and dotted contours represent easterly winds. (b) Amplitude of the modeled zonal wind power spectra over the equator for the reference simulation. Contour interval is 1 m s^{-1}.

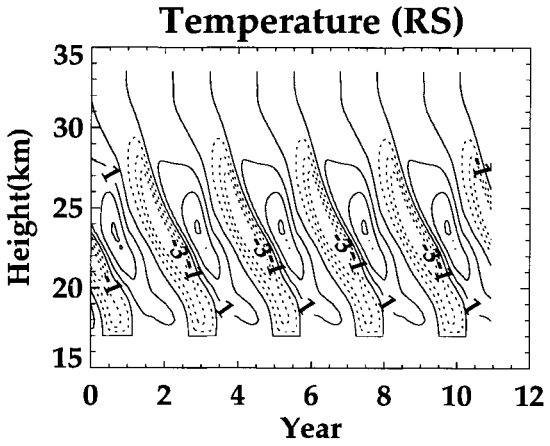

FIG. 4. Time–height cross section of modeled temperature at the equator for the RS. Contour interval is 1.0 K, and dotted contours represent negative values.

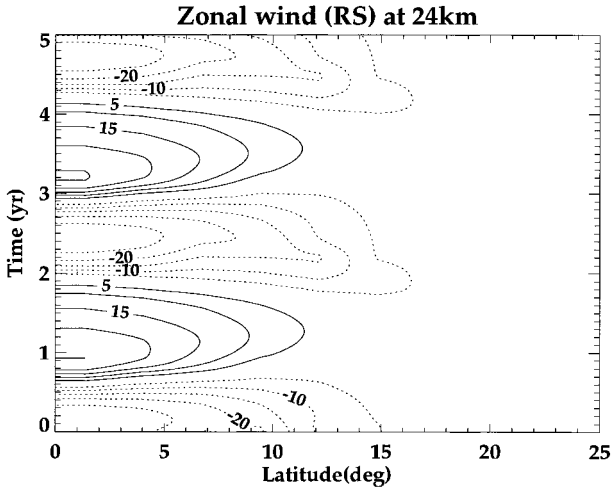

FIG. 5. Latitude–time cross section of the zonal wind at 24 km. Contour interval is 5 m s^{-1}, and dotted contours represent easterly winds.

aly ranges from about −3.5 to 3 K at the equator to about −2 to 1 K at 10°. The slightly larger cold temperature anomaly results from the stronger easterly wind shears and the larger northward heat flux associated with the Rossby–gravity wave. The modeled QBO temperature power spectrum is maximized at 1.2 K near 25-km altitude. This is in good agreement with observations from the Microwave Limb Sounder (MLS) instrument on board *UARS*, which measured a QBO temperature amplitude ranging from 1.2 to 1.6 K near 25-km altitude (Cordero et al. 1997).

The wind and temperature QBO regions descend with time in approximate agreement with observations. The westerlies descend relatively quickly between 23 and 32 km of altitude, and more slowly below 23 km. The easterlies do the opposite, descending slowly in the upper stratosphere and descending quickly in the lower stratosphere. On average, descent rates are ~0.8 km $month^{-1}$, in approximate agreement with satellite observations (Ortland et al. 1996).

Figure 5 shows a latitude–time cross section of the zonal wind at 24 km. The easterlies and westerlies are maximized near the equator, gradually diminishing with increasing latitude. In agreement with observations (Dunkerton and Delisi 1985), the easterlies extend farther from the equator than the westerlies, reaching near 15°. The ''nosing down'' of the westerlies from higher to lower levels, as originally identified by Hamiliton (1984), is also observed in the model simulations. The westerlies at upper levels (~30 km) are confined equatorward of 5°. As the westerly winds descend, they gradually spread meridionally reaching nearly 15° by 22-km altitude.

c. Ozone QBO

Figure 6 displays the time–height cross section of the ozone QBO near the equator. The maximum ozone anomaly is located between ~23- and ~26-km of altitude and ranges from −0.6 to 0.5 ppmv over the 11-yr integration. The magnitudes of the anomalies agree reasonably well with previous observations of the tropical lower stratosphere (Hasebe 1994; Cordero et al. 1997), although the vertical structures are somewhat different. However, we note that other processes not captured by our model, such as tropical–midlatitude exchange, annual variations in solar forcing, and seasonal variations in the residual circulation, may play a role in the observed ozone distribution.

Figure 7 portrays a height–latitude cross section of the QBO model simulations for day 1350 (descending easterlies) and day 1900 (descending westerlies). For the temperature field, cold anomalies are associated with strong easterly shear zones, whereas warm anomalies are associated with westerly shear zones. The vertical

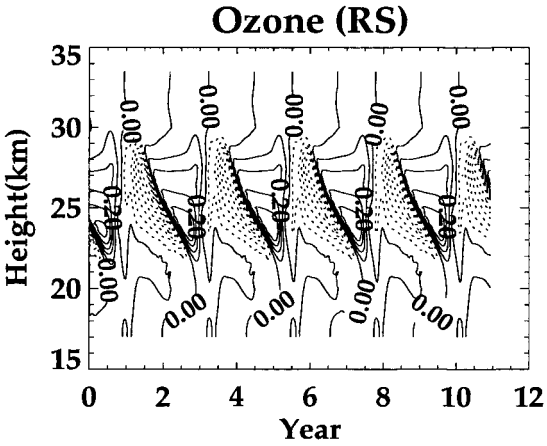

FIG. 6. Time–height cross section of modeled ozone over the equator for the RS. Contour interval is 0.1 ppmv, and dotted contours represent negative values.

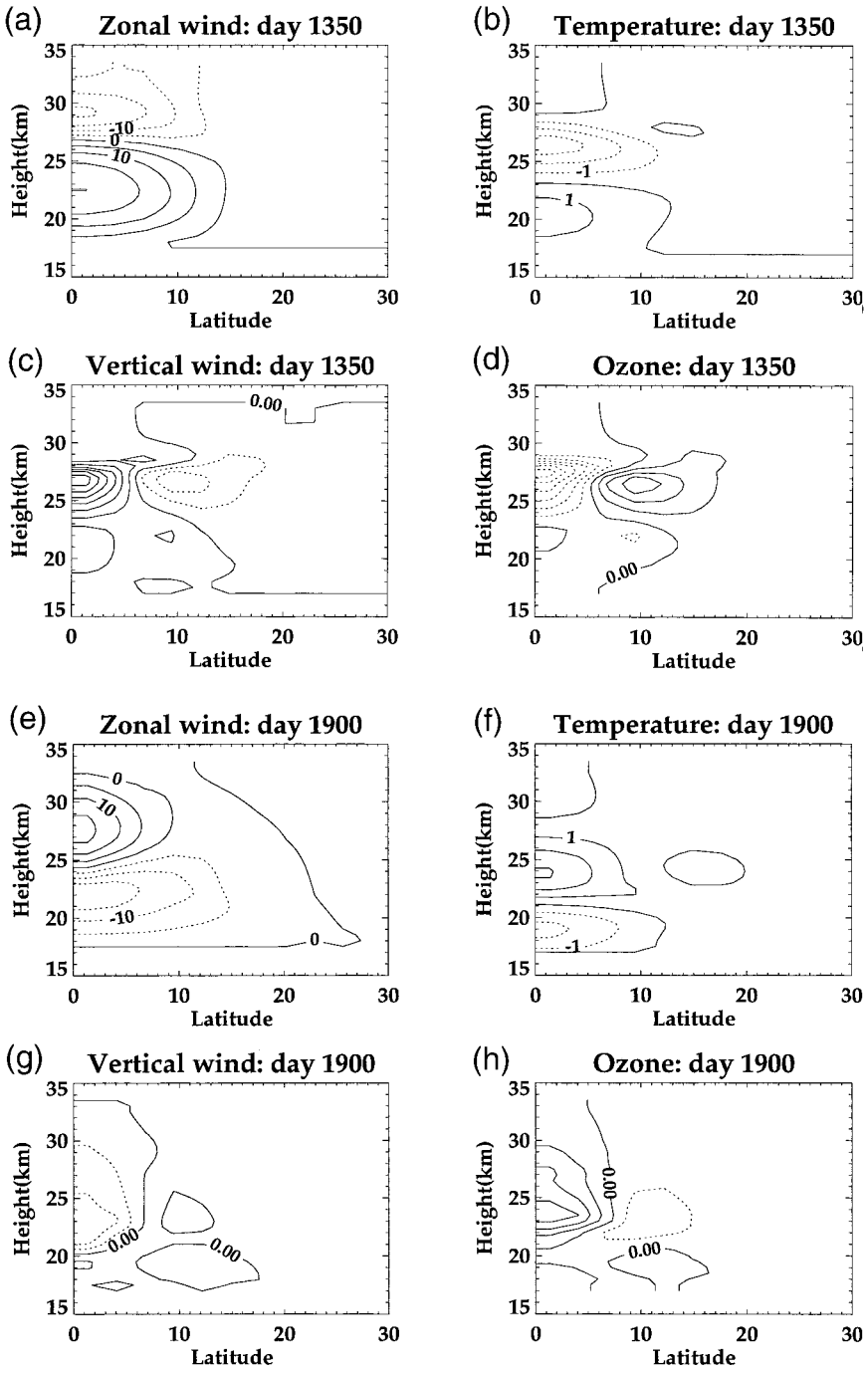

FIG. 7. Latitude–height cross section for (a)–(d) day 1350 and (e)–(h) day 1900 for (a), (e) zonal mean wind (contour interval 5 m s^{-1}); (b), (f) temperature (contour interval 1.0 K); (c), (g) vertical wind (contour interval is 0.05 mm s^{-1}); and (d), (h) zonal mean ozone volume mixing ratio (contour interval 0.1 ppmv). Dotted contours represent negative values.

motion and temperature fields are mutually consistent; that is, downward motion is required to maintain the warm anomalies that are damped by radiative cooling. The dynamically driven ozone QBO is consistent with the vertical motion field and with Plumb and Bell's (1982) conceptual model of how the QBO influences the meridional circulation of the Tropics. In particular, during descending easterlies and thus cold temperature anomalies, the upward motion transports low ozone air upward, producing a negative ozone anomaly near the equator. Poleward of the equator the reverse feature is observed, which results from the downward branch of

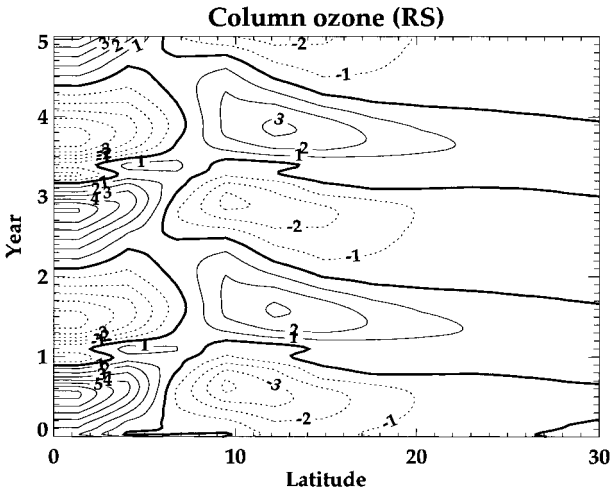

FIG. 8. Latitude–time plot of total-column ozone from the RS. The contour interval is 1 DU, and dotted contours represent negative values.

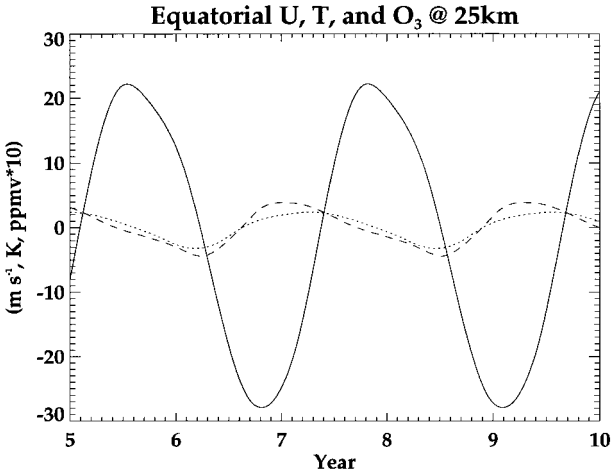

FIG. 9. Time series of zonal wind, temperature, and ozone volume mixing ratio over the equator at 25-km altitude for the RS. Zonal wind is given in m s^{-1} (solid line), temperature in K (dotted line), and ozone mixing ratio in ppmv $\times$ 10 (dashed line).

the QBO induced residual circulation. The larger negative ozone anomalies in the model are due to the stronger easterly wind shears and thus colder temperature anomalies that induce stronger upward motion near the equator.

Although the meridional structure of the *modeled* ozone QBO is similar to the symmetric circulation of Plumb and Bell (1982), the meridional structure of the *observed* ozone QBO shows seasonal variations (Tung and Yang 1994; Jones et al. 1998; Kinnersley 1999). Tung and Yang attribute these structural changes to the annual cycle. Because the present model is run for a perpetual equinox, the changes in the meridional structure of the QBO that may result from the annual cycle are excluded from consideration.

A latitude–time plot of the total column ozone (TCO) field is shown in Fig. 8. The maximum TCO ranges from -6 to 6 DU (Dobson Units) and is within the observed estimates of the tropical QBO signal ($\pm$5–10 DU) derived by Hollandsworth et al. (1995). The largest TCO anomalies occur near the equator. Smaller TCO values of opposite phase are observed away from the equator. Sufficiently far from the equator the TCO approaches zero, consistent with our lateral far-field boundary conditions. The maximum positive TCO anomalies occur at roughly the time when the maximum westerlies reach 22 km, in general agreement with observations (Hasebe 1993).

The phasing among zonal wind, temperature, and ozone in the tropical stratosphere at 25-km altitude are displayed in Fig. 9. At this level, the westerly winds reach slightly over $\sim$20 m s^{-1} while the easterlies winds reach $\sim$28 m s^{-1}. The temperature and ozone anomalies are nearly $\sim$3 K and $\sim$0.3 ppmv, respectively. The ozone and temperature fields are nearly in phase, and both lead the zonal wind by over a quarter cycle ($\sim$8 months). There is little variation in the phase among zonal wind, temperature, and ozone between 20 and 28 km over the equator. Above 30 km, ozone is primarily controlled by (temperature dependent) photochemistry rather than dynamics; thus the ozone and temperature fields are out of phase.

d. UARS observations

The above model results are now compared with *UARS* observations. We obtain zonal wind observations from the HRDI instrument, temperature observations from MLS, and ozone observations from the HALOE instrument. The HRDI winds are projected onto a 5° grid and then zonally and monthly averaged (Ortland et al. 1996). The MLS version-3 data (Fishbein et al. 1996) are binned between 4°S and 4°N and zonally averaged. The HALOE instrument uses a solar occultation sounding technique in the infrared to obtain vertical profiles of ozone and other constituents during daily sunrises and sunsets (Park et al. 1996). Because of this observing pattern, it takes nearly a month to obtain near-global coverage; thus the time series of ozone is constructed from monthly averages. Further details of the *UARS* instrument accuracy for these observations can be found in Cordero et al. (1997) and references therein. Although *UARS* began gathering observations in late 1991, aerosols from the eruption of Mt. Pinatubo significantly influenced data during 1992. Therefore, we only use data spanning the years 1993–97, which covers two full QBO cycles.

Figure 10 shows a zonally averaged time series of zonal winds, temperature anomalies, and ozone anomalies at 26 km near the equator covering the period 1993–97. The temperature and ozone anomalies were obtained by subtracting a time mean from the observations. At 26-km altitude, the zonal wind ranges from

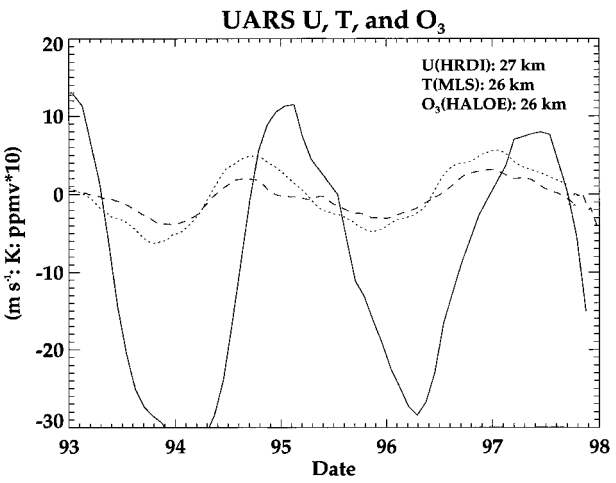

FIG. 10. Time series of the equatorial observed zonal wind (from *UARS* HRDI), and anomalies (observed value minus time mean) of temperature (from *UARS* MLS) and ozone volume mixing ratio (from *UARS* HALOE) near 26-km altitude. Zonal wind is given in m s^{-1} (solid line), temperature in K (dotted line), and ozone mixing ratio in ppmv $\times$ 10 (dashed line).

$\sim$10 to ~ -30 m s^{-1} with a period of slightly over two years. The temperature QBO leads the zonal wind oscillation by 5–6 months, or nearly a quarter period. The temperature anomaly is over 5 K during this period, which is larger than previous observations. The observed ozone anomaly, which is roughly in phase with the observed temperature anomaly, reaches almost 0.3 ppmv. In contrast to the zonal wind and temperature anomalies, the ozone anomalies are characterized by more variability. Although this may be due in part to instrument measurements, it is also likely that horizontal transport of ozone from higher latitudes may be partially responsible for some of the ozone variability.

Comparisons of the modeled time series and those from *UARS* show good agreement. The magnitude of the modeled zonal wind variations and observations are similar, although the range of values is different. The magnitudes of the temperature and ozone anomalies also compare well. Modeled ozone and temperature anomalies are approximately in phase, in agreement with observations. Hasebe (1994) notes that the in-phase relationship between the ozone and temperature QBOs can be attributed to zonal mean–ozone feedbacks. However, in our model, we obtain the observed phase relationship without any explicit ozone feedbacks.

Overall, the model simulations compare well with observations. The zonal winds and temperatures are within the range of observed values, and the structure of the ozone QBO in the Tropics is also fairly well modeled. Although the model is idealized, it contains the necessary processes to study the interactions between ozone and dynamics as outlined in the introduction. In addition, the good correspondence between the modeled fields and observations provides additional confidence in the use of this model for the analysis of ozone–dynamics interactions.

5. Ozone dynamics interactions

To understand the role ozone heating plays in the QBO, results are now presented from three model experiments. Experiment 1 allows for wave–ozone feedbacks ($A \neq 0$ in 9) but neglects the ozone QBO feedbacks ($A = 0$ in 4). Experiment 2 neglects wave–ozone feedbacks ($A = 0$ in 9) but allows for the ozone QBO feedbacks ($A \neq 0$ in 4). Experiment 3 allows for both wave–ozone and ozone–QBO feedbacks ($A \neq 0$ in 4 and 9). The results of these experiments are compared with the reference simulation (RS) which, recall, decouples the ozone heating from the dynamics ($A = 0$ in 4 and 9).

a. Wave–ozone feedbacks (expt 1)

Echols and Nathan (1996) and Cordero et al. (1998) show analytically that (linear) wave ozone feedbacks can spatially modulate forced equatorial Kelvin and Rossby–gravity waves, producing significant changes in the wave fluxes and thus the driving of the zonal mean flow.

To better understand the wave–ozone feedback process and its effect on the QBO, this section is divided into three parts: Part 1 briefly reviews the underlying theory and physical mechanisms that govern how ozone heating modulates the wave fields; part 2 presents our 2D model results, wherein the wave–ozone feedbacks alone are considered (i.e., the ozone QBO is neglected); and part 3 calculates the Eliassen–Palm flux and corresponding zonal mean body force that results from the wave–ozone feedbacks.

1) THEORETICAL BASIS

Following Leovy's (1966) reasoning regarding the photochemical destabilization of mesospheric gravity waves, the linear, vertical spatial modulation of equatorial waves due to wave–ozone feedbacks can be understood as follows. In regions where the background ozone volume mixing ratio *increases* with altitude, wave-induced downward (upward) displacements of ozone rich (poor) air produce local diabatic heating (cooling). For such wave-induced perturbations, it can be shown that the vertical velocity and temperature fields are in phase. Therefore, vertical velocity and temperature are positively correlated, which is associated with the transformation of wave potential energy to wave kinetic energy and thus wave amplification.

For example, Echols and Nathan (1996) and Cordero et al. (1998) have shown that for slowly varying background fields and weak diabatic heating, the local spatial damping rate of the Kelvin wave can be written as

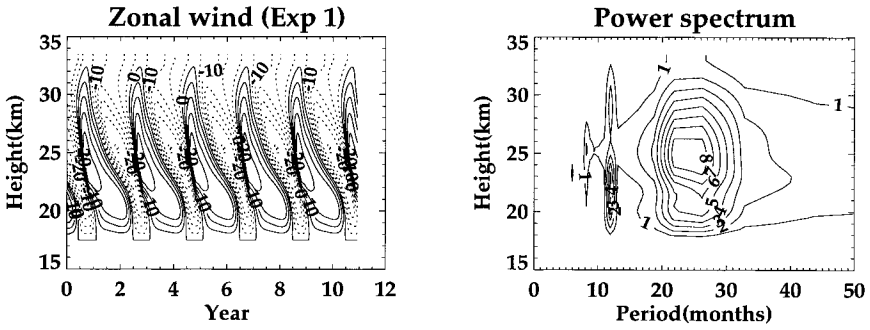

FIG. 11. As in Fig. 3, except for expt 1.

$$m_i = -\frac{N}{2k_K c_K^2}\left[\alpha_N - \frac{A\overline{\gamma}_z}{N^2}\right]. \quad (15)$$

Thus in the equatorial stratosphere below (above) ~35 km, where $\overline{\gamma}_z > 0$ (<0), the vertical ozone advection reduces the damping due to Newtonian cooling and is thus destabilizing (stabilizing). An expression similar to (15) can also be derived for the Rossby–gravity wave.

2) NUMERICAL RESULTS

Experiment 1 examines the effects of wave–ozone feedbacks on the QBOs in zonal mean wind, temperature, and ozone. Generally, the feedbacks have their greatest impact on the zonal mean temperature field, with a lesser impact on the zonal wind and ozone fields.

A time–height cross section of the zonal wind QBO at the equator for expt 1 is shown in Fig. 11. Although the time–height structure of the oscillation and strength of the zonal winds at the equator are similar to the RS (see Fig. 3a), there are several important differences. For example, the westerly shear zones between 22 and 26 km are more pronounced than in the RS, and the QBO period is reduced from 26 months in the RS to 24 months. At 12° latitude between 22- and 30-km altitude, the westerly winds are weaker by ~2 m s^{-1} (30%) compared to the RS, whereas the easterly winds are stronger by ~1 m s^{-1} (5%).

There are also significant changes in the temperature QBO between expt 1 and the RS. For example, near the equator, the temperature QBO increases by ~0.5K (~20%). The positive temperature anomaly increases from 3.0 to 3.5 K near 23 km, whereas the negative temperature anomaly decreases only slightly between 20 and 30 km. As distance from the equator increases, the differences between expt 1 and the RS decrease. The temperature changes due to the wave–ozone feedbacks can also be seen in the ozone distribution. Compared to the RS, the ozone QBO amplitude in expt 1 is over 10% larger between 22 and 27 km throughout the Tropics.

3) ELIASSEN–PALM FLUX

The zonal mean body force per unit mass ($\Im$) produced by the divergence of EP flux provides an effective measure of the wave driving of the zonal mean circulation. Integrating over a meridional cross section, $\Im$ can be written as (Andrews et al. 1987)

$$\langle \nabla \cdot \mathbf{F} \rangle = \frac{\partial \langle F_z \rangle}{\partial z} = \frac{\partial}{\partial z}\rho\left(\frac{\beta y}{N^2}\overline{v'\phi'_z} - \overline{u'v'}\right), \quad (16)$$

where $\mathbf{F}$ is the EP flux vector, $\langle\ \rangle = L^{-1}\int_{-\infty}^{\infty} dy$, and L = 1200 km is the meridional scale of the QBO.

To provide greater understanding of how wave ozone feedbacks affect the QBO, we calculate $\Im$ for zonal mean wind profiles corresponding to different phases of the QBO. Figure 12 compares $\langle\Im\rangle$ from the RS and expt 1 at day 1900, when descending westerly winds of the QBO are observed in the middle stratosphere. During this period, the maximum EP flux for the Kelvin wave occurs near the maximum westerly shear zone, at approximately 25 km in altitude. The wave–ozone feedbacks (expt 1) yield wave amplitudes that are up to 10% larger than the RS, resulting in a stronger driving of the zonal mean circulation. During the descending easterly phase of the QBO (not shown), the maximum EP flux due to the Rossby–gravity wave occurs near the strong easterly shear zones, and again, wave–ozone feedbacks increase the wave driving by 5%–10%. These results are consistent with the studies of Echols and Nathan (1996) and Cordero et al. (1998), which showed that EP fluxes are enhanced by the heating due to wave–ozone feedbacks.

b. Zonal mean–ozone feedbacks (expt 2)

Experiment 2, which examines the diabatic heating effects of the ozone QBO on the zonal mean circulation [$A \neq 0$ in Eq. (4); $A = 0$ in Eq. (9)], shows that the diabatic effects of the ozone QBO produce significant changes in the zonal wind, temperature, and ozone distributions. The results from expt 2 are summarized in Fig. 13, which shows a time–height cross section of the equatorial zonal wind and the corresponding power

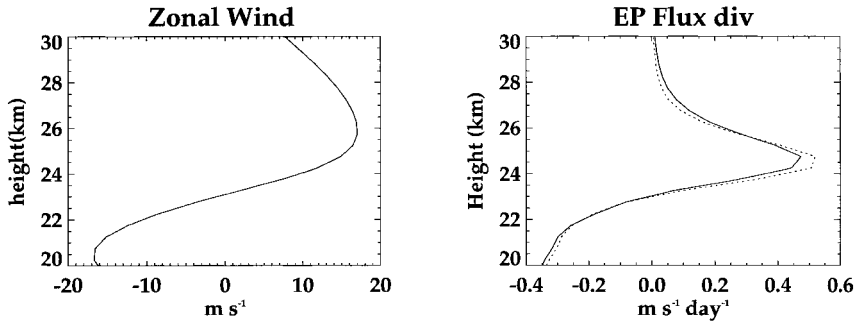

FIG. 12. (a) Zonal wind at the equator on day 1900 in m s^{-1}. (b) Vertical profile of the latitudinally integrated density weighted EP flux divergence (m s^{-1} day^{-1}), calculated using the basic-state profile from day 1900. The solid lines denote calculations made from the RS, and the dashed lines denote calculations made from expt 1.

spectrum. The ozone QBO increases the maximum amplitude of the zonal wind by ~1–2 m s^{-1} and reduces the oscillation period by ~1 month. Like expt 1, the maximum westerly shear zones are stronger compared to the RS. Away from the equator, the zonal winds are ~10% larger then the RS and the difference between the easterly and westerly wind regimes is enhanced. Similar changes in the zonal wind QBO due to the ozone QBO have been obtained by Li et al. (1995).

The amplitude of the temperature QBO is ~20% larger than the RS within 0°–15° latitude. The warm anomalies are most affected by the ozone QBO, increasing at the equator from ~3 K in the RS to ~4 K in expt 2. Correspondingly, zonal mean ozone anomalies also increase in expt 2 from ~10% at the equator to ~30% elsewhere. The larger ozone anomalies are due to a stronger meridional circulation. For example, in expt 2, the amplitude of the zonal mean vertical motion field increases by over 10% near the equator and by over 25% at the poleward flanks of the Tropics. This is a positive feedback, whereby the ozone QBO increases the magnitude of the temperature QBO, thus producing a larger-amplitude ozone QBO.

These results at first seem to contradict Hasebe (1994), who suggests that the diabatic influence of the ozone QBO will reduce the meridional circulation of the QBO. However, because the RS and expt 2 have different zonal wind shears and temperatures, we cannot directly compare the meridional circulations of these simulations. Moreover, Hasebe's model is unable to capture how the zonal mean–ozone feedbacks affect the zonal mean wind, temperature, and ozone distributions.

Because the wave fields are sensitive to the background distribution of temperature and zonal wind, changes in the temperature QBO due to the diabatic feedbacks of the ozone QBO are not independent of the driving-wave fields. Nevertheless, to better isolate the effects of the ozone QBO on the meridional circulation, we compare simulated QBOs of roughly equal strength with and without the ozone feedbacks. This is accomplished by running the expt 2 simulation with reduced wave amplitudes, producing a QBO that has a similar vertical wind shear and temperature to that of the RS. This enables a direct comparison of the mean meridional circulation for simulations with and without zonal mean–ozone feedbacks. We find that by reducing the wave-forcing amplitudes of the Kelvin and Rossby–gravity waves by about 9% (zonal mean ozone feedbacks are included), we can produce a QBO of roughly equal strength as the RS. Although the vertical wind shear and temperature are of roughly equal strength, the QBO period for the reduced wave forcing case is almost six months longer than the RS. However, in the context of studying the meridional circulation, the length of the QBO period is not important.

A comparison of the two QBO simulations indicates

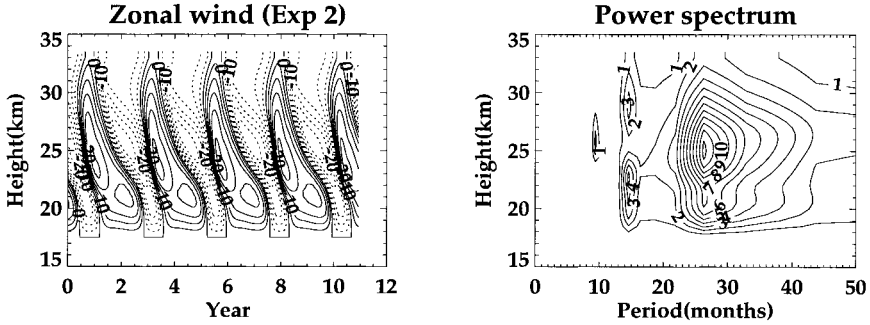

FIG. 13. As in Fig. 3, except for expt 2.

TABLE 2. Range of values for the QBO in zonal wind, temperature, and ozone volume mixing ratio at the equator and at 12° latitude for the RS and the three experiments. The period of the QBO is calculated using the zonal wind at the equator.

		Equator			12° Latitude		
Case	Period	U (m s^{-1})	T (K)	O_3 (ppmv)	U (m s^{-1})	T (K)	O_3 (ppmv)
Reference	28 months	$26 \rightarrow -30$	$3 \rightarrow -4.8$	$0.5 \rightarrow -0.7$	$4 \rightarrow -15$	$1.5 \rightarrow -1.1$	$0.35 \rightarrow -0.2$
Expt 1	25 months	$24 \rightarrow -30$	$3.6 \rightarrow -4.6$	$0.54 \rightarrow -0.7$	$3 \rightarrow -16$	$1.5 \rightarrow -1.2$	$0.37 \rightarrow -0.22$
Expt 2	29 months	$27 \rightarrow -33$	$3.6 \rightarrow -5.3$	$0.55 \rightarrow -0.75$	$3.5 \rightarrow -18$	$1.4 \rightarrow -1.1$	$0.45 \rightarrow -0.25$
Expt 3	28 months	$27 \rightarrow -34$	$4.6 \rightarrow -5.0$	$0.58 \rightarrow -0.75$	$4.5 \rightarrow -20$	$1.6 \rightarrow -1.2$	$0.47 \rightarrow -0.28$

that zonal mean–ozone feedbacks reduce the strength of the mean meridional circulation. In particular, when zonal mean–ozone feedbacks are included, the vertical motion field is 15% weaker in amplitude compared to the RS. A smaller reduction in the strength of the zonal mean ozone QBO is also observed. As previously explained, the additional diabatic heating produced by the ozone QBO partially offsets the heating required to maintain thermal wind balance in the presence of radiative cooling. Thus, in areas of westerly wind shear, downward transport of ozone will elevate the radiative equilibrium temperature so that less vertical motion will be required to maintain the temperature perturbation against radiative damping.

To summarize this section, the zonal mean ozone changes are due to two feedback processes, one direct and the other indirect. First, the diabatic feedbacks of the ozone QBO reduces the QBO induced meridional circulation, which *directly* changes the zonal mean ozone field. Second, the diabatic feedbacks of the ozone QBO results in changes in the wind and temperature fields, which in turn alters the absorption properties of the driving waves, which *indirectly* changes the zonal mean ozone field. The net result of the indirect changes is stronger zonal wind shears and temperature gradients, which are maintained by an enhanced meridional circulation. This wave-enhanced meridional circulation more than offsets the changes in the meridional circulation due to the diabatic heating effects of the ozone QBO.

c. Full ozone coupling (expt 3)

Experiment 3 (expt 3) includes the diabatic heating produced by both wave–ozone and zonal mean–ozone feedbacks [$A \neq 0$ in Eqs. (4) and (9)]. Generally, expt 3 is a combination of the results from expt 1 and expt 2. The results obtained at the equator for the three experiments are summarized in Table 2. Briefly, the QBO period is reduced by the wave–ozone feedbacks, increased by the zonal mean–ozone feedbacks, and resides between these results for full ozone coupling. The amplitude of the zonal wind, temperature, and ozone QBO variations follows a similar pattern.

The minimum and maximum temperature and ozone anomalies at the equator during the last five years of integration for the RS and three experiments are displayed in Fig. 14. The largest differences are found between 22- and 27-km altitude. The maximum temperature anomaly increases from 3.0 to 3.5 K (20%) when either wave ozone–feedback or zonal mean–ozone feedbacks are included. The ozone-induced temperature anomalies increase to over 4.5 K (~50%) when both ozone feedbacks are included. Significant changes in the maximum ozone distribution are also evident in Fig. 14.

The ozone feedbacks also produce significant circulation changes away from the equator. For example, at 12° latitude the easterly phase of the QBO is stronger in all three experiments (see Fig. 15), whereas the westerly winds are generally weaker. With full ozone coupling the maximum easterlies (westerlies) reach 20 m s^{-1} (3.5 m s^{-1}), an increase (decrease) of over 30% (10%) compared to the RS. The magnitude of the ozone and temperature variations also increases at 12° latitude (not shown): the amplitude of the ozone QBO increases by nearly 0.1 ppmv (~25%); the amplitude of the temperature QBO increases by less than <10%. These increases are evident within ~15° of the equator and indicate the importance of ozone feedbacks on the circulation and structure of the QBO.

The effects of the ozone feedbacks on the amplitude of the QBO at the equator and at 12° latitude are summarized in Fig. 16. At the equator, wave–ozone feedbacks generally increase by <10% the amplitude of the zonal wind, temperature, ozone, and vertical-motion QBOs. The heating due to the zonal mean–ozone (ozone QBO) feedbacks has a larger impact (~20%) on the QBOs in wind, temperature and ozone. The combination of wave–ozone and zonal mean–ozone feedbacks increases the magnitude of the QBOs by 10%–25% over the RS. Similar results are found near 12°, where full ozone feedbacks increase the magnitude of the QBOs by ~10%–40%.

6. Summary and conclusions

The effects of both wave and zonal mean ozone heating feedbacks on the quasi-biennial oscillation (QBO) were investigated using a mechanistic model of the lower equatorial stratosphere. The model atmosphere, which accounts for wave–mean but not wave–wave interactions, is represented by zonal mean and linear wave descriptions of the ozone, temperature, and wind fields. The model circulation is driven by Kelvin and Rossby–gravity waves at the lower boundary.

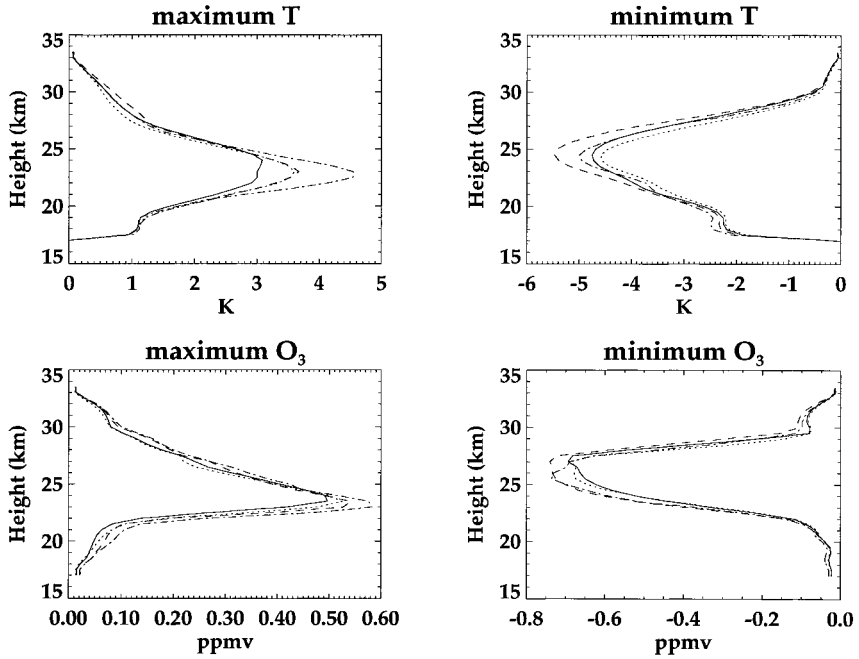

FIG. 14. Comparison of minimum and maximum values of (a), (c) temperature; and (b), (d) ozone during the last five years of integration at the equator. The solid lines denote the RS, whereas the dotted, dashed, and dot–dashed lines refer to expt 1, expt 2, and expt 3, respectively.

A reference simulation (RS) of the QBO, in which ozone feedbacks are neglected, yields results that are in good agreement with *Upper Atmosphere Research Satellite* observations. The RS is then used as a basis for comparison with three model experiments, which examine separately and in combination the effects of wave–ozone and zonal mean–ozone feedbacks.

Wave–ozone feedbacks alone (expt 1) increase the wave driving of the zonal mean flow by up to 10%. This enhanced wave driving produces stronger shear zones in the zonal wind QBO, and an increase in the magnitude of the temperature and ozone QBOs by ~10%–20%. These results agree with the analytical studies of Echols and Nathan (1996) and Cordero et al. (1998), which show that the wave–ozone feedbacks increase the equatorial wave amplitudes, thus increasing the zonal mean acceleration.

Like the wave–ozone feedbacks, the zonal mean–ozone feedbacks also influence the dynamical QBO by similar magnitudes, albeit via different mechanisms. Alone, the diabatic feedbacks of the ozone QBO decrease the induced meridional circulation by nearly 15%. However, because wave absorption is sensitive to the zonal mean wind and temperature distributions, diabatic feedbacks of the QBO alter the mean temperature distribution and thus change the wave absorption properties of the driving waves. The zonal mean–ozone feedbacks increase the amplitudes of the temperature and ozone QBOs by ~10%–30%. The stronger temperature QBO, induced by the diabatic feedbacks of the ozone QBO, produces a more vigorous circulation.

The combined effects of wave–ozone and zonal mean–ozone feedbacks reinforce each other, thus increasing further the circulation strength of the QBO.

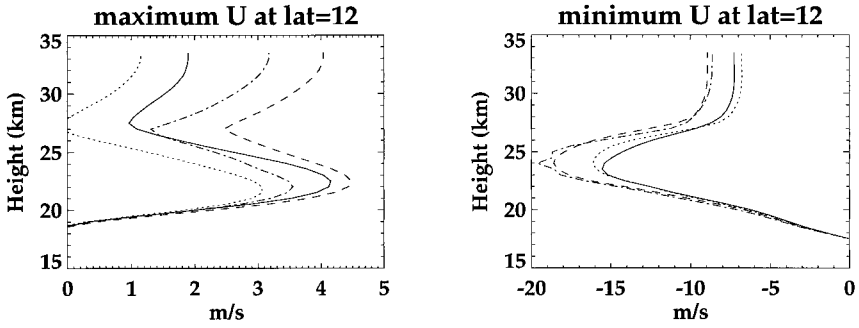

FIG. 15. As in Fig. 14, except for the zonal wind at 12° latitude.

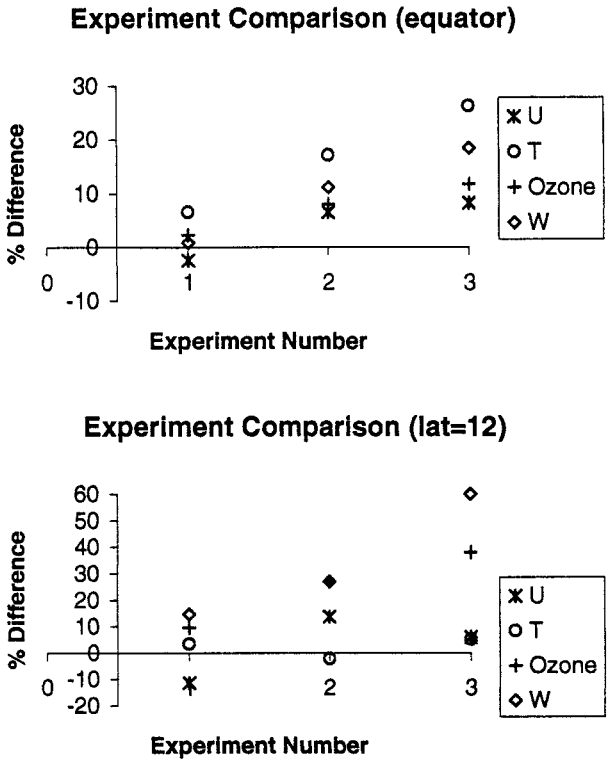

FIG. 16. Comparison between the amplitudes at the equator and 12° latitude for the QBO variations in zonal wind, temperature, ozone volume mixing ratio, and vertical motion; these fields are calculated as a percent difference from the reference simulation. Percent difference for expt 1 calculated as $100(X_{\text{Exp1}} - X_{\text{ref}})(X_{\text{ref}})^{-1}$.

Near the equator, the amplitudes of the zonal wind and temperature QBOs are ~10%–20% larger than the model simulations without the ozone feedbacks. Even larger changes are observed away from the equator (e.g., 12° latitude), where the strength of the meridional circulation increases by up to 30%. The combined ozone feedbacks have little influence on the period of the QBO. However, it is important to note that because of the stronger meridional circulation, smaller wave amplitudes can be used to drive the QBO. Model sensitivity experiments indicate that when ozone feedbacks are included, wave amplitudes can be reduced by ~10% and still maintain a QBO circulation similar to the RS.

Because the modeled QBO fields of zonal wind, temperature, and ozone agree well with satellite and in situ observations, the model is an excellent tool for carrying out mechanistic studies of the tropical lower stratosphere. However, there are improvements that can be made to the model, thus allowing a broader scope of study. For example, extending the model's vertical domain into the upper stratosphere would allow a more detailed study of the two-cell structure of the ozone QBO and its potential feedbacks on the zonal mean circulation. In addition, imposing a realistic tropical ascent rate would allow the study of the interaction of the QBO (and associated meridional circulation) with the seasonally varying tropical ascent rate, and how ozone feedbacks may alter these interactions.

A final point worth noting is that mechanistic models of the QBO require enhanced wave amplitudes to drive the circulation. The amplitudes of the Kelvin wave and especially the Rossby–gravity wave are larger than observed estimates (Takahashi and Boville 1992). Recent model simulations indicate that small-scale gravity waves are a likely source of additional momentum needed to drive the dynamical QBO (Dunkerton 1997). Thus a broadening of the wave spectrum may provide additional understanding of how the wave ozone feedbacks impact the zonal mean circulation.

Acknowledgments. The authors thank Kristien King for assisting in the numerical calculations. The authors also thank Dr. Masaaki Takahashi for his helpful suggestions and for providing the source code for the dynamical portion of the model. This work was supported by the National Aeronautics and Space Administration (Grants NAG8-871, NAG8-1054, NAG8-1143, and Training Grant NGT-30153) and the University of California Institute for Collaborative Research (INCOR). Partial support has also been provided for ECC through the *UARS* Guest Investigator Program.

APPENDIX

Specification of Ozone Wave Structure at the Lower Boundary

Given the geopotential height distributions for the Kelvin and Rossby–gravity waves at the lower boundary [(12) and (13)], wave solutions for the horizontal and vertical velocities, temperature, and ozone volume mixing ratio can be obtained there. Briefly, the meridional velocity and temperature at the lower boundary are obtained by solving (7) and (9) and applying the result at the lower boundary. The perturbation vertical velocity does not need to be specified at the boundary; rather, we calculate it directly from the continuity equation, which we integrate downward from the upper boundary. To calculate the perturbation ozone volume mixing ratio, we consider the Kelvin and Rossby–gravity waves separately. For the Kelvin wave, (10) yields,

$$\gamma_t' = -w'\overline{\gamma}_z, \tag{A1}$$

$$\frac{\partial \Phi_z'}{\partial t} + N^2 w' = 0, \tag{A2}$$

where we have neglected the radiative–photochemical effects relative to the dynamical effects, which is an excellent approximation in the lower stratosphere, that is, near the lower boundary at 17 km. Also, we have set $\overline{u} = \overline{\Phi}_z = 0$ (at lower boundary) and noted that for the Kelvin wave $v' \approx 0$. Combining (A1) and (A2) yields

$$\gamma' = \frac{\overline{\gamma}_z \Phi'_z}{N^2}. \quad \text{(A3)}$$

A similar analysis can be carried out for the Rossby–gravity wave. In particular, noting that

$$v' = ik\Phi'(\beta y)^{-1}, \quad \text{(A4)}$$

we obtain from (10) the ozone perturbation for the Rossby–gravity wave,

$$\gamma' = \frac{\overline{\gamma}_z \Phi'_z}{N^2} + \frac{\overline{\gamma}_y \Phi'}{c_R \beta y}. \quad \text{(A5)}$$

REFERENCES

Andrews, D. G., J. R. Holton, and C. B. Leovy, 1987: *Middle Atmosphere Dynamics.* Academic Press, 489 pp.

Bowman, K. P., 1989: Global patterns of the quasi-biennial oscillation in total ozone. *J. Atmos. Sci.,* **46,** 3328–3343.

Chipperfield, M. P., L. J. Gray, J. S. Kinnersley, and J. Zawodny, 1994: A two-dimensional model study of the QBO signal in SAGE II NO_2 and O_3. *Geophys. Res. Lett.,* **21,** 589–592.

Cordero, E. C., S. R. Kawa, and M. R. Schoeberl, 1997: An analysis of tropical transport: Influence of the quasi-biennial oscillation. *J. Geophys. Res.,* **102,** 16 453–16 461.

——, T. R. Nathan, and R. S. Echols, 1998: An analytical study of ozone feedbacks on Kelvin and Rossby-gravity waves: Effects on the QBO. *J. Atmos. Sci.,* **55,** 1051–1062.

Dunkerton, T. J., 1983: Laterally-propagating Rossby waves in the easterly acceleration phase of the quasi-biennial oscillation. *Atmos.–Ocean,* **21,** 55–68.

——, 1985: A two-dimensional model of the quasi-biennial oscillation. *J. Atmos. Sci.,* **42,** 1151–1160.

——, 1997: The role of gravity wave in the quasi-biennial oscillation. *J. Geophys. Res.,* **102,** 26 053–26 076.

——, and D. P. Delisi, 1985: Climatology of the equatorial lower stratosphere. *J. Atmos. Sci.,* **42,** 376–396.

——, and ——, 1997: Interaction of the quasi-biennial oscillation and stratopause semiannual oscillation. *J. Geophys. Res.,* **102,** 26 107–26 116.

Echols, R. S., and T. R. Nathan, 1996: Effects of ozone heating on forced equatorial Kelvin waves. *J. Atmos. Sci.,* **53,** 263–275.

Fels, S. B., 1982: A parameterization of scale-dependent radiative damping rates in the middle atmosphere. *J. Atmos. Sci.,* **39,** 1141–1152.

Fishbein, E. F., and Coauthors, 1996: Validation of UARS Microwave Limb Sounder temperature and pressure measurements. *J. Geophys. Res.,* **101,** 9983–10 016.

Fleming, E. L., S. Chandra, M. R. Schoeberl, and J. J. Barnett, 1988: Monthly mean global climatology of temperature, wind, geopotential height and pressure for 0–120 km. NASA Tech. Memo. 100697, 85 pp.

Funk, J. F., and G. L. Garnham, 1962: Australian ozone observations and a suggested 24 month cycle. *Tellus,* **14,** 378–382.

Hamiliton, K., 1984: Mean wind evolution in the tropical lower stratosphere. *J. Atmos. Sci.,* **41,** 2113–2125.

Hartmann, D. L., and R. R. Garcia, 1979: A mechanistic model of ozone transport by planetary waves in the stratosphere. *J. Atmos. Sci.,* **36,** 350–364.

Hasebe, F., 1994: Quasi-biennial oscillations of ozone and diabatic circulation in the equatorial stratosphere. *J. Atmos. Sci.,* **51,** 729–745.

Hollandsworth, S. M., K. P. Bowman, and R. D. McPeters, 1995: Observational study of the quasi-biennial oscillation in ozone. *J. Geophys. Res.,* **100,** 7347–7361.

Holton, J. R., and R. S. Lindzen, 1972: An updated theory for the quasi-biennial cycle of the tropical stratosphere. *J. Atmos. Sci.,* **29,** 1076–1080.

Huang, T. Y., 1996: The impact of solar radiation on the quasi-biennial oscillation of ozone in the tropical stratosphere. *Geophys. Res. Lett.,* **23,** 3211–3214.

Jones, D. B. A., H. R. Schneider, and M. B. McElroy, 1998: Effects of the quasi-biennial oscillation on the zonally averaged transport of tracers. *J. Geophys. Res.,* **103,** 11 235–11 249.

Keating, G. M., and D. F. Young, 1985: *Middle Atmosphere Program Handbook for MAP,* University of Illinois, 318 pp.

Kinnersley, J. S., 1999: Seasonal asymmetry of the low- and middle-latitude QBO circulation anomaly. *J. Atmos. Sci.,* **56,** 1140–1153.

Leovy, C. B., 1966: Photochemical destabilization of gravity waves near the mesosphere. *J. Atmos. Sci.,* **23,** 223–232.

Li, D., K. P. Shine, and L. J. Gray, 1995: The role of ozone-induced diabatic heating anomalies in the quasi-biennial oscillation. *Quart. J. Roy. Meteor. Soc.,* **121,** 937–943.

Lindzen, R. S., 1971: Equatorial planetary waves in shear: Part I. *J. Atmos. Sci.,* **28,** 609–622.

——, and C. Y. Tsay, 1975: Wave structure of the tropical stratosphere during 1 April–30 July 1958. *J. Atmos. Sci.,* **32,** 2008–2021.

Ling, X.-D., and J. London, 1986: The quasi-biennial oscillation of ozone in the tropical middle stratosphere: A one-dimensional model. *J. Atmos. Sci.,* **43,** 3122–3137.

McPeters, R. D., D. F. Heath, and P. K. Bhartia, 1984: Average ozone profiles for 1979 from the NIMBUS 7 SBUV instrument. *J. Geophys. Res.,* **89,** 5199–5214.

Nathan, T. R., 1989: On the role of ozone in the stability of Rossby normal modes. *J. Atmos. Sci.,* **46,** 2094–2100.

——, and L. Li, 1991: Linear stability of free planetary waves in the presence of radiative-photochemical feedbacks. *J. Atmos. Sci.,* **48,** 1837–1855.

——, E. C. Cordero, and L. Li, 1994: Ozone heating and the destabilization of traveling waves during summer. *Geophys. Res. Lett.,* **21,** 1531–1534.

Naujokat, B., 1986: An update of the observed quasi-biennial oscillation of the stratospheric winds over the Tropics. *J. Atmos. Sci.,* **43,** 1873–1877.

Ortland, D. A., W. R. Skinner, P. B. Hays, M. D. Burrage, R. S. Lieberman, A. R. Marshall, and D. A. Gell, 1996: Measurements of stratospheric winds by the high resolution Doppler imager. *J. Geophys. Res.,* **101** (D6), 10 351–10 363.

Park, J. H., and Coauthors, 1996: Validation of Halogen Occultation Experiment CH_4 measurements from the UARS. *J. Geophys. Res.,* **101,** 10 183–10 203.

Plumb, A. R., and R. C. Bell, 1982: A model of the quasi-biennial oscillation on an equatorial beta-plane. *Quart. J. Roy. Meteor. Soc.,* **108,** 335–352.

Ramanathan, K. R., 1963: Bi-annual variation of atmospheric ozone over the tropics. *Quart. J. Roy. Meteor. Soc.,* **89,** 540–542.

Randel, W. J., and F. Wu, 1996: Isolation of the ozone QBO in SAGE II data by singular-value decomposition. *J. Atmos. Sci.,* **53,** 2546–2559.

Reed, R. J., 1964: A tentative model of the 26-month oscillation in tropical latitudes. *Quart. J. Roy. Meteor. Soc.,* **90,** 441–466.

——, W. J. Campbell, L. A. Rasmussen, and D. G. Rogers, 1961: Evidence of downward propagating annual wind reversal in the equatorial stratosphere. *J. Geophys. Res.,* **66,** 813–818.

Salby, M. L., D. L. Hartmann, P. L. Bailey, and J. C. Gille, 1984: Evidence for equatorial Kelvin modes in *Nimbus-7* LIMS. *J. Atmos. Sci.,* **41,** 220–235.

Stolarski, R. S., and A. R. Douglass, 1985: Parameterization of the photochemistry of stratospheric ozone including catalytic loss process. *J. Geophys. Res.,* **90,** 10 709–10 718.

Takahashi, M., 1987: A 2-dimensional numerical model of the quasi-biennial oscillation: Part I. *J. Meteor. Soc. Japan,* **65,** 523–536.

——, and J. R. Holton, 1991: The mean zonal flow response to Rossby wave and gravity wave forcing in the equatorial lower stratosphere: Relationship to the QBO. *J. Atmos. Sci.,* **48,** 2078–2087.

——, and B. A. Boville, 1992: A three-dimensional simulation of

the equatorial quasi-biennial oscillation. *J. Atmos. Sci.,* **49,** 1020–1035.

Tung, K. K., and H. Yang, 1994: Global QBO in circulation and ozone. Part I: Reexamination of observational evidence. *J. Atmos. Sci.,* **51,** 2699–2707.

Veryard, R. G., and R. A. Ebdon, 1961: Fluctuations in tropical stratospheric winds. *Meteor. Mag.,* **90,** 125–143.

Wallace, J. M., 1973: General circulation of the tropical lower stratosphere. *Rev. Geophys. Space Phys.,* **11,** 191–222.

——, and V. E. Kousky, 1968: Observational evidence of Kelvin waves in the tropical stratosphere. *J. Atmos. Sci.,* **25,** 900–907.

Yanai, M., and T. Maruyama, 1966: Stratospheric wave disturbances propagating over the equatorial Pacific. *J. Meteor. Soc. Japan,* **44,** 291–294.

Zawodny, J. M., and M. P. McCormick, 1991: Stratospheric aerosol and gas experiment II measurements of the quasi-biennial oscillation in ozone and nitrogen dioxide. *J. Geophys. Res.,* **96,** 9371–9377.

Zhu, X., and J. R. Holton, 1986: Photochemical damping of inertia-gravity waves. *J. Atmos. Sci.,* **43,** 2578–2584.